International Journal of Physical Sciences Vol. 7(8), pp. 1286 - 1293, 16 February, 2012
Available online at http://www.academicjournals.org/IJPS
DOI: 10.5897/IJPS11.887
ISSN 1992 - 1950 ©2012 Academic Journals

Full Length Research Paper

Simulation and experimental work on manufacturing torispherical heads in explosive hydro-forming process

S. Jabalamelian* and Aidy Ali

Department of Mechanical and Manufacturing Engineering, Universiti Putra Malaysia, 43400 UPM, Serdang, Selangor, Malaysia.

Accepted 30 January, 2012

This study presents a numerical investigation on the deformation of the circular blanket against a male die under impulsive loading to form a torispherical heads shape. A finite element model was developed and verified with experimental tests for the explosive forming of the torispherical heads made of AA5083 aluminum alloy in the framework of LS-DYNA crash simulator software. The nature of the deformation was turned from the stretching to the buckling and compression of the specimen by using a male die, which is a novel concept in the high speed forming processes. Johnson-Cook (JC) and Modified Zerilli-Armstrong (MZA) constitutive equations were used to describe the behavior of the specimen in a high strain rate forming process with different stress status. Most of the experimentally observed material behaviors simulated well in pure tension or compression tests, while the transient zone was not adequately described. The predicted width for the transient rim is considerably smaller than experimental measurements. The blast loading process including the underwater detonation and the interaction with the specimen simulated using Arbitrary Lagrangian-Eulerian formulation as well as cavitations and reloading effect. The simulation results for blast loading verified base on Cole's relation for the underwater detonation of small charges, show a good agreement of 95% accuracy.

Key words: Explosive hydro-forming, male die, arbitrary Lagrangian-Eulerian formulation, torispherical head, Johnson-Cook, Zerilli-Armstrong.

INTRODUCTION

Impulsive forming processes that contribute large deformation at the strain rates above 10^3 s^{-1} and temperatures as high as 0.6 melting points such as explosive forming method (EFM), electro magnetic forming (EMF), electro hydraulic forming (EHF) and recently invented Laser Shock Forming (LSF) have been extensively studied and documented well since 1950s. However, the application of these methods have not been expanded from the academic lab or high tech. industries to the mass production to date (Tekkaya and Allwood, 2011). Mynors and Zhang (2002) described some of the noteworthy applications of impulsive loading methods in real industrial projects and investigated the potential reasons to explain why these techniques are abandoned by the commercial industries. The lack of the fundamental knowledge and the straightforward numerical simulation techniques to eliminate costly, time consuming trial and error experimental works are the two most promising explanations. As Verleysen et al. (2011) stated, even a clear method to determine the forming limit diagrams (FLDs) of materials in a high speed forming process has not been established yet.

Fortunately, a large number of studies have been conducted to investigate the effects of strain rate and temperature on the forming behavior of materials in a few past years. Kim et al. (2011) used nuiaxial tensile test to assess the effects of strain rate to the formidability of the auto-body steel sheets. Similar works have been performed for magnesium alloy by Ulacia et al. (2011), for titanium alloy by EL-Domiaty (1992), for tungsten alloy by Rohr et al. (2008) and for aluminum alloys by Chen et al.

*Corresponding author: E-mail: saeed_jabalamelian@yahoo.com. Tel: +60 13-2682064.

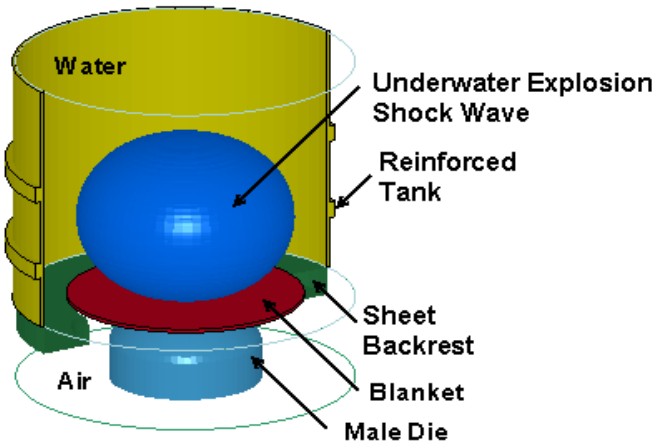

Figure 1. Explosive hydro-forming set configuration.

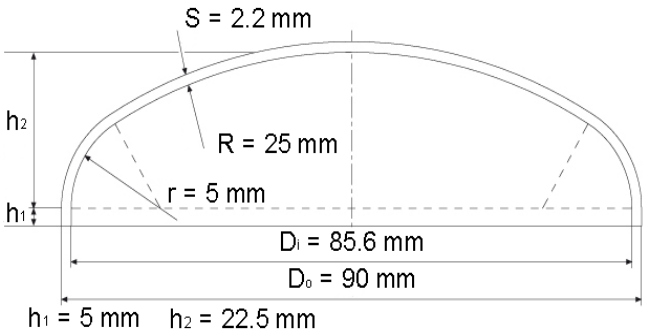

Figure 2. Final product configuration.

(2009) and Smerd et al. (2005). The results of these studies are usually fitted to the previously developed strain rate and temperature sensitive constitutive equations for the specified range of strain rate and temperature to determine material constants. These constants would vary even for the same material by fitting the constitutive model over the data with the different range of temperatures and strain rates.

The growing request to application of aluminum alloy in automotive and aerospace industries has brought great interests in understanding and modeling the behavior of these alloys in quasi-static, high strain rate and super plasticity regime. However, a large portion of previously done researches were concentrated on tension stress status such as the works performed by Toros and Ozturk (2010) and Zhang et al. (2010). Clausen et al. (2004) investigated the flow stress of the AA5083 through uniaxial tensile tests in three different directions of the rolled plate material with the strain rate, and temperature varies from 5×10^5 to 50 s^{-1} and 20 to 250˚C, respectively. In this study, most of the material behaviors were represented by JC model except the negative strain rate sensitivity that requires special attentions. Gao et al. (2009) also studied the effect of stress status based on stress triaxiality and load angle. Another comprehensive study on the plasticity characteristics of the AA5083 aluminum alloy under tension, compression and torsion stress status for the stain rates as high as 10^3 s^{-1} was carried out by Tucker et al. (2010). To the authors' knowledge, no study has been performed on transient stress states up to now. In the present study, the experimental tests and numerical simulations are conducted to investigate the behavior of the AA5083 circular sheet in a high strain rate procedure involving tension, compression and transient stress status.

EXPERIMENTAL PROCEDURES

The 140 mm diameter circular blankets were cut from 2.2 mm thick AA5083 aluminum alloy sheet that was processed by annealing. The stress-strain relation was investigated for the instance from the same sheet plate by uniaxial tensile test which revealed the yield stress of 151 MPa, ultimate stress of 320 MPa and fracture stress of 301 MPa. The corresponding strain for the ultimate and fracture stress were found to be 30.0 and 31.5%, respectively. Concentric circles with the 10 mm gap were finely machined on the top surface of specimens to represent the hoop strain. The thickness strain was measured with caliper after destructive test. An inner curved sheet backrest was employed to hold the blanket over the die with 5 mm gap. A spherical charge made from 8.15 g composition C4 fixed above the center of the blanket at the standoff distance of 50 mm, detonated by the standard igniter number 8 in the depth of 220 mm of water that is high enough to eliminate the effects of the reflected wave from the surface on the deformation process. The C4 has the density of 1.601 g/cm^3, detonation velocity of 0.804 cm/μs and the detonation pressure of 0.281 Mbar. The water container was a 300 mm high reinforced steel tank with the diameter of 220 mm (Figure 1).

The desired final product is similar to 2:1 torispherical dished head in the ASMI code for one exception (Ellenberger et al., 2004). The radius of the inner curve is two times greater than the thickness that is considerably smaller than proposed value in the standard design. This sharp bend limit the transient stress status zone to a narrow distinct rim which is more convenient to investigate (Figure 2).

THE MODELING PROCEDURE

The modeling of the underwater explosion

Due to rapid large change between the boundary of materials and traveling mass of one material inside the others, it is not adequate to apply ordinary finite element or finite difference methods to simulate underwater detonation though it was practiced before. As another option, Wijayathunga and webb (2006) introduced the following relation for the actual pressure acting on the deformation instead to model the real explosion.

$$p(t) = 2p_0 \exp[-\frac{1}{\theta}(t-\frac{Q}{\upsilon_w})] - \rho_c \upsilon_p \quad (1)$$

where Q is the difference between the shortest distance and the

Table 1. Grunesien parameters for water, air and AA5083.

Parameter	Water	Air	AA5083
C [cm/μs]	0.14830	0.14800	0.39400
γ_0	1.20000	0.28000	2.02000
a	0.00000	0.00000	0.47000
S_1	2.10570	1.75000	1.49800
S_2	-0.17440	0.00000	0.00000
S_3	0.010085	0.00000	0.00000

distance to the point that is considered on the loaded surface, v_m is the speed of the pressure wave, p_0 and θ are constants dependent on charge weight and standoff distance. In this study, ALE multi-material formulation was adopted to model the underwater detonation as well as the motion of the blanket in the water/air medium. As Alia and Souli (2006) described, in this method the finite element meshes are provided to move independently from the material flow and each element can contain a mixture of two or more different materials. On the other hand, in the ALE approach, two meshes can overlap each other, one is the background mesh which can move arbitrary in the space and the other is attached to the material which flows through the former moving mesh. The material is deform in the Lagrangian step and distributed back onto the moving reference ALE mesh. Explosives, air and water were modeled with 8 and 6 node finite elements using high explosive burn and null material models, both require an equation of state. The JWL (Jones-Wilkins-Lee) equation of state was employed to determine the relation between the pressure and volume of the detonation products, which is defined as follows (Alia and Souli 2006):

$$p_{JWL} = A\left(1-\frac{\omega}{R_1 V}\right)\exp(-R_1 V) + B\left(1-\frac{\omega}{R_2 V}\right)\exp(-R_2 V) + \frac{\omega}{V}E \quad (2)$$

where A, B, R_1, R_2 and ω are constant and E is the internal energy density per initial volume unit. The C4 JWL parameters are as follows: A = 5.98155, B = 0.13750, R_1 = 4.5, R_2 = 1.5, E = 0.087 Mbar and ω = 0.32. The following form of Mie-Gruneisen equation of state with cubic shock velocity- particle velocity (v_s-v_p) defines pressure for the water and air.

$$P = \frac{\rho_0 C^2 \mu\left[1+\left(1-\frac{\gamma_0}{2}\right)\mu - \frac{a}{2}\mu^2\right]}{\left[1-(S_1-1)\mu - S_2\frac{\mu^2}{\mu+1} - S_3\frac{\mu^3}{(\mu+1)^2}\right]^2} + (\gamma_0 + a\mu)E \quad (3)$$

Here C is the interception of the v_s-v_p curve, S_1, S_2 and S_3 are the coefficient of the slope of the same curve, γ_0 is the Gruneisen gamma, a is the first order volume correction to γ_0 and μ=(ρ/ρ$_0$)-1. The following nonlinear v_s-v_p was proposed by Steinberg (1987).

$$v_s = 0.148 + 2.56 v_p - 1.986\left(\frac{v_p}{v_s}\right)v_p + 0.2268\left(\frac{v_p}{v_s}\right)^2 v_p \quad (4)$$

The Grunesien parameters for water, air and AA5083 are given in Table 1.

The modeling of the blanket

The blanket was modeled with thick shell 4 node finite elements using JC and MZA constitutive equations completed with Grunesien equation of state. The JC equation describe the von mises stress flow stress as follows (Johnson and Cook, 1983):

$$\sigma = [A + B\varepsilon^n][1 + C\ln\dot{\varepsilon}_p][1 - T^{*m}] \quad (5)$$

where the ε is the equivalent plastic strain, $\dot{\varepsilon}_p$ is the dimensionless plastic strain rate for $\dot{\varepsilon}_0$ = 1.0 s^{-1}, the T^* is the homologous temperature and the A, B, C, n and m are material constants.

$$\dot{\varepsilon}_P = \frac{\dot{\varepsilon}}{\dot{\varepsilon}_0} \quad (6)$$

$$T^* = \frac{T - T_{room}}{T_{melt} - T_{room}} \quad (7)$$

The expression in the first set of brackets give the stress as a function of strain, including combination of yield and strain hardening portion, for $\dot{\varepsilon}_p$ = 1 and T^* = 0. The second and the third set of brackets represent the effect of strain rate and temperature, respectively. According to Gray et al. (1994), the JC parameters for AA5083 at high strain rate forming are as follows: A = 170 MPa, B = 425 MPa, n = 0.42, C = 0.0335, m = 1.225 and T_m = 933°K.

The MZA model presents a more physically based constitutive equation which is coming from dislocation mechanics concepts with the following expression:

$$\sigma = C_1 + C_2\varepsilon^n \exp(-C_3 T + C_4 T\ln\dot{\varepsilon})\frac{\mu(T)}{\mu(298)} \quad (8)$$

In which ε, $\dot{\varepsilon}$ and T represent the strain, strain rate and absolute temperature respectively and C_1 to C_4 and n are material constants, which were determined for AA5083 as C_1 = 91 MPa, C_2 = 805 MPa, C_3 = 0.00145, C_4 = 0.00007 and n = 0.265 by Gray et al. (1994). The temperature dependency on flow stress yield is as follows.

$$\frac{\mu(T)}{\mu(298)} = \frac{1.13691 - 0.16332}{\exp(234/T) - 1} \quad (9)$$

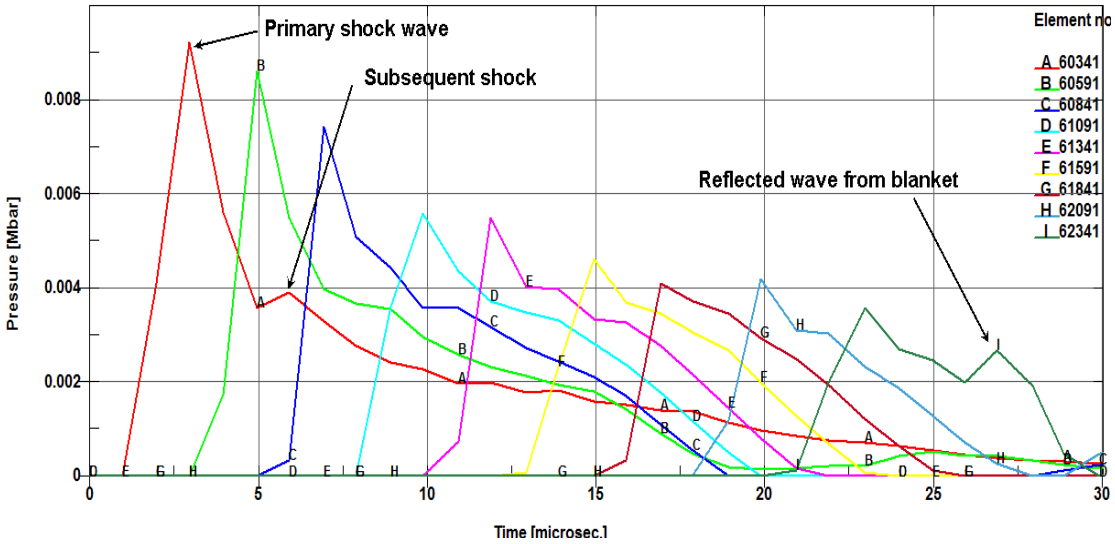

Figure 3. Pressure time history for nine different standoff distances.

Boundary conditions

For the common boundaries between the explosive and water or between water and air is not necessary to define any specific contact or coupling. But in these boundaries, which materials flow from one region of the mesh to another, the common nods should be merged. The intersection between the blanket as a Lagrangian part and the water or air as the ALE regions have to be defined with coupling boundary conditions, while the contact between the blanket and the die, as another Lagrangian part, can simply be modeled by forming surface to surface or any other contact. Generally, when a Lagrangian part hits another lagrangian object, it is required to define a contact. Conversely, when a Lagrangian part hit an ALE region, coupling should be defined between two parts. Moreover, in order to avoid initial air leakage from the ALE mesh, one bar pressure is exposed to the air section boundaries.

SIMULATION RESULTS AND DISCUSSION

Underwater detonation

Underwater explosion is briefly described as a chemical reaction which breaks down the original explosive molecules into solid and gas product materials.

Consequently, a superheated, high compressed gas bubble would be generated. The rapid expansion of the solid charge into high compressed gas bubble will generate a shock wave in the surrounding water which propagates toward the work piece with the velocity of sound. As the bubble expand, its inner pressure would reduce to less than the surrounding pressure which lead to contraction of the bubble. But the contraction increases the inner pressure of the bubble once again until another expansion would occurred. On the other hand, buoyancy forces the bubble to move upward, but the cycle of expansion - contraction would repeat several times before reaching the surface and each cycle would produce its own shock wave (Rajendran and Narasimhan, 2006). Four distinct shocks wave were recognized in current simulation including primary 500 MPa and subsequent 100, 70 and 50 MPa shock waves respectively. Previously, comprehensive experimental and theoretical studies were carried out by Cole (1948) to represent a mathematical model for underwater explosion. He described the pressure time history for any fixed location in the standoff distance, S, from the explosive charge in the water medium as an exponential function shown as follows (Rajendran and Narasimhan, 2006):

$$p(t) = P_m e^{-\frac{t}{\theta}} \quad (10)$$

where θ is the decay time and P_m is the peak pressure; both depend on the size of the charge and standoff distance.

$$P_m = 52.16\left(\frac{W^{1/3}}{S}\right)^{1.13} \quad (11)$$

$$\theta = 96.5(W^{1/3})\left(\frac{W^{1/3}}{S}\right)^{-0.22} \quad (12)$$

W is the mass of the charge that is expressed in kg of TNT. But this formulation just approximates an instantaneous increase to the peak pressure, P_m, after a holdup time. This relation includes neither the immediate decay occurring after the rapid increase, nor the effects of subsequent shocks (Figure 3). Hence, Cole's

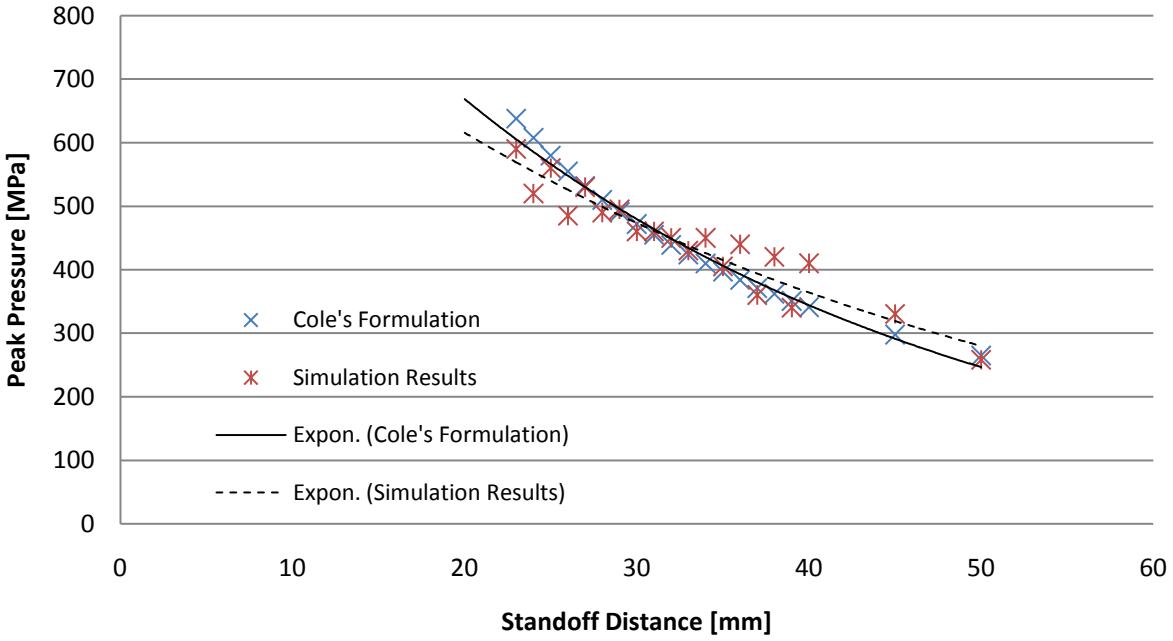

Figure 4. Peak pressure for different standoff distances in water medium according to Cole's formulation and simulation results.

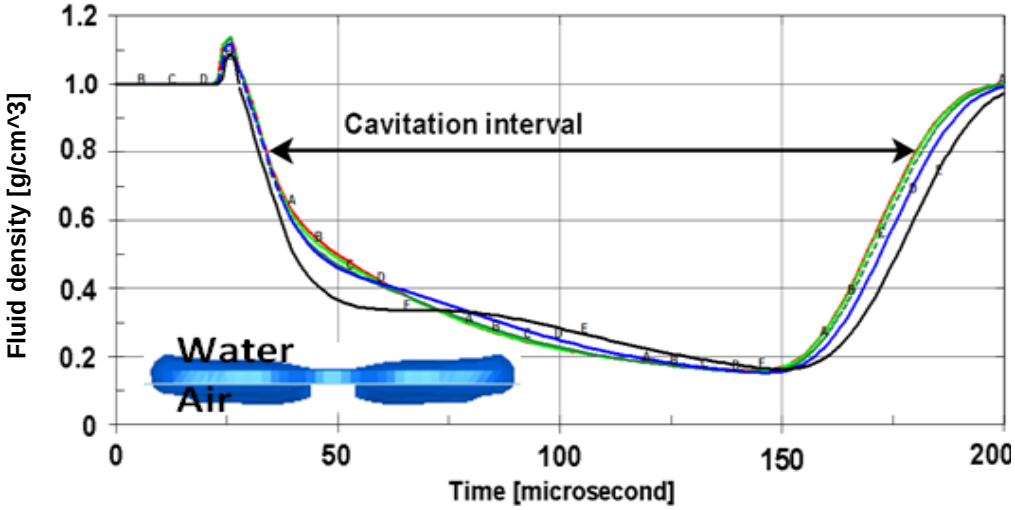

Figure 5. Density time history for cavitated area.

formulation is not well accurate in the vicinity of the explosive charge (ten times the charge radius) while it is adequate enough elsewhere (Figure 4).

Investigating the cavitations and reloading effect

As the primary shock is transmitted to the blanket, it gets modified by accelerating of the plate and reflected back into water. The downward motion of the blanket while the liquid is simultaneously subjected to follow upwards by the reflected wave can reduce the pressure to below vapor pressure that causes cavitations. Cavitations begin immediately after the primary shock wave impinges the blanket and continued until the secondary shock reaches the cavitated area. In this study, the cavitations emerged as low pressure zone shown in Figure 5. But there is no evidence to prove that this zone occupied with either gas, liquid or mixture of both. Therefore, both the density and the pressure for selected elements inside the low

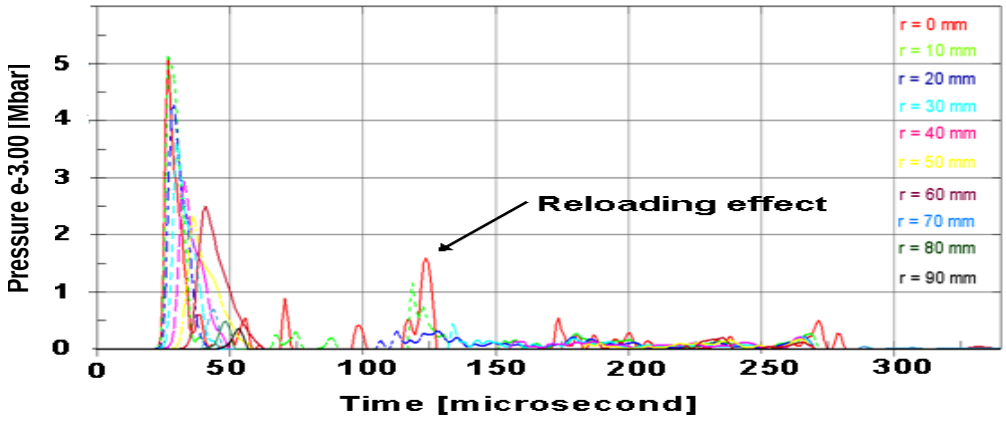

Figure 6. Pressure profile acting over the blanket.

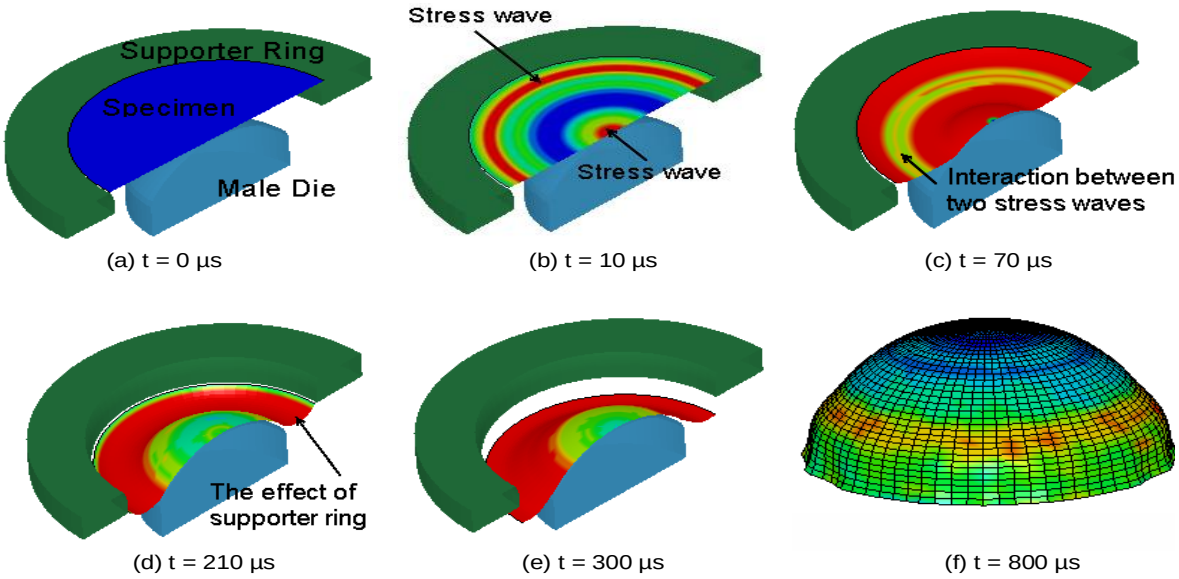

Figure 7. Deformation process for a specimen from the second group.

pressure zone were extracted to determine the water situation according to super heated water thermodynamic charts (Wylen et al., 2002). The energy transition established once again after cavitations which is known as reloading effect or water hummer reloading and delivers even more energy to the blanket than primary shock wave (Rajendran and Narasimhan, 2006). Although this succeeding loading has a major role in forming process, it is hard to control and can result in ruptured blanket. Also the tremendously high temperature of the cavitated zone can ruin the quality of the diaphragm's surface. Since forming the cavitations is not avoidable in many of the EHF process, it has tried to decrease the interval of cavitations as much as possible. One of the most advantageous of male die comparing with female matrix or free forming method is shifting the cavitated zone from central parts to the sides as displayed in Figure 3. Moreover, the cavitations interval for forming the similar work pieces through free forming method is between 500 to 2500 µs as Mousavi et al. (2007) stated, but in our proposed method the cavitations interval reduced to less than 180 µs. The pressure time history of water element located above the sheet metal is illustrated in Figure 6.

Investigating the strain distribution

The predicted sequence of deformed configurations of AA5083 blanket is shown in Figure 7. The results show

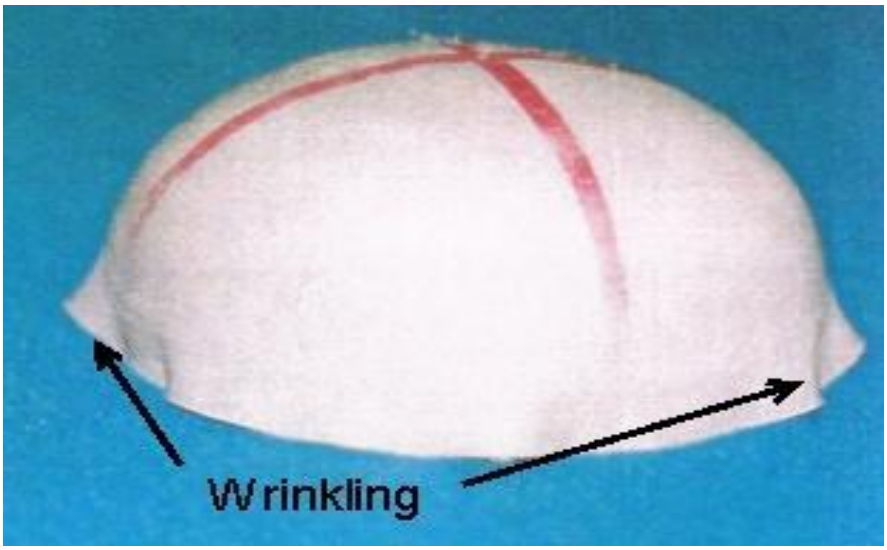

Figure 8. Experimentally formed specimen.

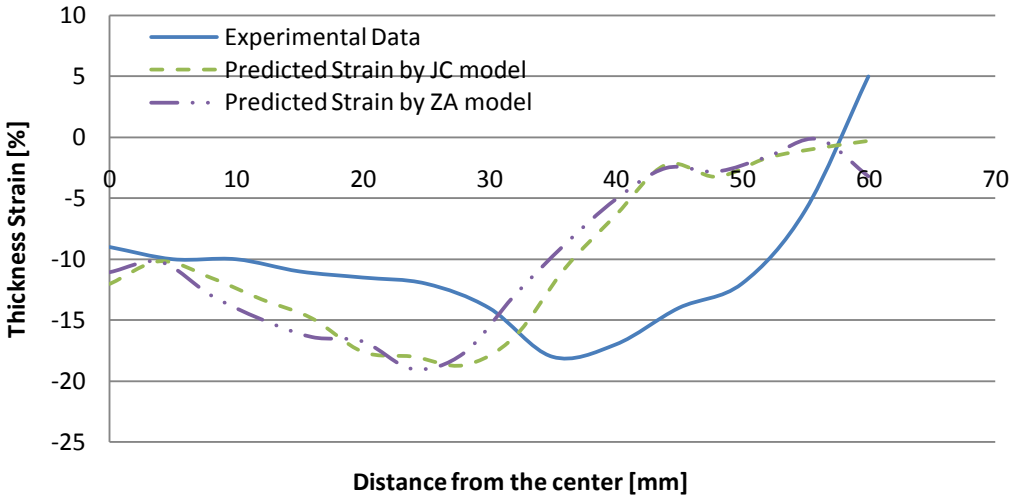

Figure 9. Thickness strain distribution base on experimental tests, JC and MZA constitutive models.

two stress waves, one initiate at the rim and move toward the center while the other propagates peripherally from the center. Both the central part and rim undergo pure tension stress status until the stress fronts collide with each other. After the collision, the stress status in the rime has been changed to the compression and it has continued to deform in the buckling mode. Hence, a transient stress status region can be supposed next to the collision rime that is traveling toward the edge of blanket (Figure 8).

Figure 9 reveals that both JC and MZA constitutive equations expect similar thickness strain distribution, which is reasonably in good agreement with experimental measurements. But a 10 mm shift between the simulation results and the experimental data is observed which is referred to the infirmity of the currently available constitutive equations to model transient stress status.

Conclusion

A simulating approach to model the especially design explosive hydro-forming process for manufacturing torispherical dished head by using male die has been developed. The authenticity of the simulation results was evaluated base on corresponding experimental test and

other previously done experimental and theoretical investigation. The impulsive loading including the main loading, subsequent loading and reloading effects has been modeled using ALE multi-material formulation. It is in a good agreement of 95% with Cole's experimentally developed relation for underwater detonation of small charge.

The behavior of the AA5083 circular blanket under impulsive loading reasonably well predicted with the JC and MZA constitutive equations and Mie - Grunesien equation of state in pure tension and compression stress status. However, none of them can model the transient stress situation adequately.

REFERENCES

Alia A, Souli M (2006). High explosive simulation using multi-material formulations. Appl. Therm. Eng., 26(10): 1032-1042.

Chen Y, Clausen AH, Hopperstand OS, Langseth M (2009). Stress-strain behavior of aluminum alloys at a wide range of strain rates. Int. J. Solids Struct., 46(21): 3825-3835.

Clausen AH, Børvik T, Hopperstand OS, Ahmed B (2004). Flow and fracture characteristics of aluminum alloy AA5083-H116 as function of strain rate, temperature and triaxiality. Mater. Sci. Eng., A364(1-2): 260-272.

Cole HR (1948). Underwater Explosion. New Jersey: Prinveton University Press. NJ, 437 p.

El-Domiaty A (1992). The effect of strain, strain rate and temperature on formability of Ti-6Al-4V alloy. J. Mater. Process. Technol., 32(1-2): 243-251.

Ellenberger JP, Chuse R, Carson B (2004). Pressure vessels: the ASME code simplified. Columbus: McGraw-Hill Professional, pp. 47-73.

Gao X, Zhang T, Hayden M, Roe C (2009). Effects of the stress state on plasticity and ductile failure of an aluminum 5083 alloy. Int. J. Plasticity, 25(12): 2366-2382.

Gray GT, Chen SR, Wright W, Lopez MF (1994). Constitutive Equation for Annealed Metals Under Compression at High Strain Rates and High Temperatures. New Mexico: los Alamos National Laboratory, pp. 21-28.

Johnson GR, Cook WH (1983). A constitutive Model and data for metals subjected to large strains, high strain rates and high temperatures. Hague: Seventh International Symposium on Ballistics, pp. 541-547.

Kim SB, Huh H, Bok HH, Moon MB (2011). Forming limit diagram of auto-body steel sheets for high-speed sheet metal forming. J. Mater. Process. Technol., 211(5): 851-862.

Mynors DJ, Zhang B (2002). Applications and capabilities of explosive forming. J. Mater. Process. Technol., 125-126: 1-25.

Rajendran R, Narasimhan K (2006). Deformation and fracture behavior of plate specimens subjected to underwater explosion - A review. Int. J. Impact Eng., 32(12): 1945-1963.

Rohr I, Nahme H, Thoma K, Anderson CE (2008). Material characterization and constitutive modeling of a tungsten-sintered alloy for a wide range of strain rates. Int. J. Impact Eng., 35(8): 811-819.

Smerd R, Winkler S, Salisbury C, Worswick M, Lloyd D, Finn M (2005). High strain rate tensile testing of automotive aluminum alloy sheet. Int. J. Impact Eng., 32(1-4): 541-560.

Steinberg DJ (1987). Spherical explosion and the equation of state of water. Livermore: Lawrence Livermore National Laboratory (LLNL), pp. 3-7.

Tekkaya AE, Allwood JM (2011). Impulse forming. J. Mater. Process. Technol., 211(5): 785-786.

Toros S, Ozturk F (2010). Modeling uniaxial, temperature and strain rate dependent behavior of Al-Mg alloys. Cmp. Mat. Sci., 49(2): 333-339.

Tucker MT, Horstemeyer MF, Whittington WR, Solanki KN, Gullett PM (2010). The effect of varying strain rates and stress states on the plasticity, damage, and fracture of aluminum alloys. Mech. Mater., 42(10): 895-907.

Ulacia I, Salisbury CP, Hurtado I, Worswick MJ (2011). Tensile characterization and constitutive modeling of AZ31B magnesium alloy sheet over wide range of strain rates and temperatures. J. Mater. Process. Technol., 211(5): 830-839.

Verleysen P, Peirs J, Slycken JV, Faes K, Duchene L (2011). Effect of strain rate on the forming behavior of sheet metals. J. Mater. Process. Technol., 211(8): 1457-1464.

Wijayathunga VN, Webb DC (2006). Experimental evaluation and finite element simulation of explosive forming of a square cup from a brass plate assisted by a lead plug. J. Mater. Process. Technol., 172(1): 139-145.

Wylen V, Sonntag, Borgnakke (2002). Fundamentals of Thermodynamics. New York: Wiley and Sons Inc., pp. 682-687.

Zhang C, Leotoing L, Guines D, Ragneau E (2010). Experimental and numerical study on effect of forming rate on AA5086 sheet formability. Mater. Sci. Eng. A., 527(4-5): 967-972.